Magnetism of Fe^{2+} ions in $Cd_{1-x}Fe_xTe$ compounds

C. Testelin, C. Rigaux, A. Mauger, and A. Mycielski*
Groupe de Physique des Solides, Universités Paris VI et VII, Tour 23, 2 place Jussieu, 75251 Paris CEDEX 05, France

M. Guillot
Service National des Champ Intenses, Centre National de la Recherche Scientifique, Boîte Postale 166 X, 38042 Grenoble CEDEX, France

(Received 13 June 1991)

Magnetization measurements up to 20 T have been performed on $Cd_{1-x}Fe_xTe$ ($x=0.018$ and 0.033), at temperatures between 1.6 and 20 K, for different crystallographic directions. A theoretical computation involving the diagonalization of the Hamiltonian of an isolated Fe^{2+} ion subjected to crystal-field, spin-orbit, and Zeeman terms within the lowest ^5D manifold gives the main features of the magnetization curves. In particular, this model predicts the magnetic anisotropy observed at low temperature, for $B > 5$ T, but does not reproduce the low-temperature magnetization at high fields. We show that a quantitative agreement can be achieved only if the Fe-Fe spin interaction is taken into account. The exchange interaction between an isolated ion and all the other ions beyond nearest neighbors (NN) is treated in a mean-field approximation. The NN interaction is treated separately, by exact diagonalization of the pair Hamiltonian in a truncated matrix. Under the assumption of a random distribution of magnetic ions, a quantitative agreement with experiments is achieved for two investigated compositions and for the different crystallographic directions. From this analysis, we determine both the NN and the molecular-field exchange constants.

I. INTRODUCTION

The outstanding physical properties of Fe-based semimagnetic semiconductors[1,2] are related to the d^6 electronic configuration of Fe^{2+} ions which possess both orbital and spin angular momentum ($L=2, S=2$). The effects of the crystal field and spin-orbit interaction on a Fe^{2+} isolated ion in II-VI compounds have been studied theoretically;[2-5] they have also been explored experimentally through optical measurements, such as Raman scattering in $Cd_{1-x}Fe_xSe$,[6] and infrared absorption in $Cd_{1-x}Fe_xTe$.[3] A quantitative agreement between theory and experiments has been found for $Cd_{1-x}Fe_xSe$.[6] We have argued in the preceding paper (hereafter referred to as paper I) that such an agreement is also achieved in $Cd_{1-x}Fe_xTe$, provided that we take into account the dynamic Jahn-Teller coupling between the phonons and the iron electronic states involved in transitions originating from the ^5E ground multiplet. This quantitative agreement between theory and optical measurements is evidence that the electronic structure of isolated Fe^{2+} ions is well determined within the crystal-field model.

The magnetic properties of these materials are also sensitive to the electronic structure of Fe^{2+}: in II-VI compounds, Fe^{2+} generates a Van Vleck type of paramagnetism since the ground state of Fe^{2+} is the nonmagnetic singlet of symmetry Γ_1. The contribution of isolated Fe^{2+} ions, as it is computed from the above-mentioned crystal-field model, is sufficient to reproduce the main features of the magnetization curves, both for $Cd_{1-x}Fe_xSe$ (Refs. 7 and 8) and for $Cd_{1-x}Fe_xTe$.[9] This model, however, fails to give quantitative agreement with the low-temperature magnetization at high fields, and overestimates, for example, the saturation of the magnetization curves. Since this model gives an accurate description of the electronic structure of isolated ions, the deviation between theoretical and experimental magnetization curves must result from Fe-Fe magnetic interactions. The investigation of these interactions is the purpose of the present work, in which we report an extensive study, both experimental and theoretical, of the magnetization in $Cd_{1-x}Fe_xTe$. The measurements have been made at temperatures between 1.6 and 20 K on oriented single crystals, in the range of composition $x < 0.04$, for magnetic fields up to 20 T applied along different principal directions of the cubic crystal. Experimental data are presented in Sec. III. We show that quantitative agreement between theory and experiment is achieved if the Fe-Fe spin interaction, assumed to be of the Heisenberg type, is taken into account. The model is reported in Sec. IV. The exchange interaction between one ion and all the other ions beyond nearest neighbors (NN) is treated in the mean-field approximation. The NN interaction is treated separately, by exact diagonalization of the pair Hamiltonian in a truncated basis. The final section is devoted to the application of the model to fit the experimental data, from which we derive the NN and the molecular-field exchange constants.

II. EXPERIMENTS

Single crystals of $Cd_{1-x}Fe_xTe$ have been grown by a Bridgman method. The crystal structure has been controlled by x-ray diffraction. The Fe concentration x (always smaller than 0.04) has been measured by microprobe analysis. Highly homogeneous single crystals

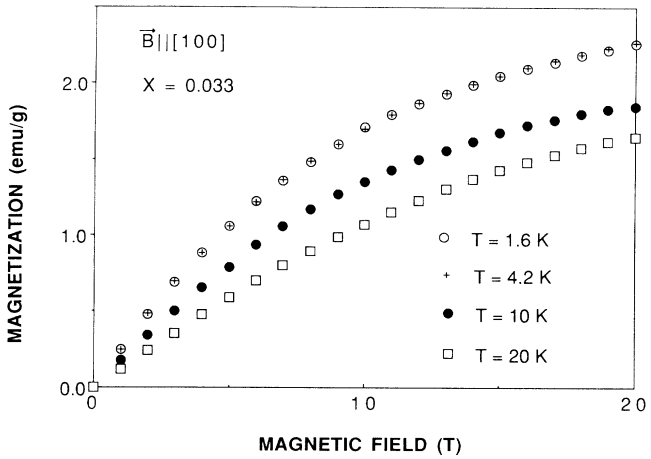

FIG. 1. Experimental magnetization of $Cd_{1-x}Fe_xTe$ ($x=0.033$) at $T=1.6$, 4.2, 10, and 20 K, for $\mathbf{B}\|[100]$.

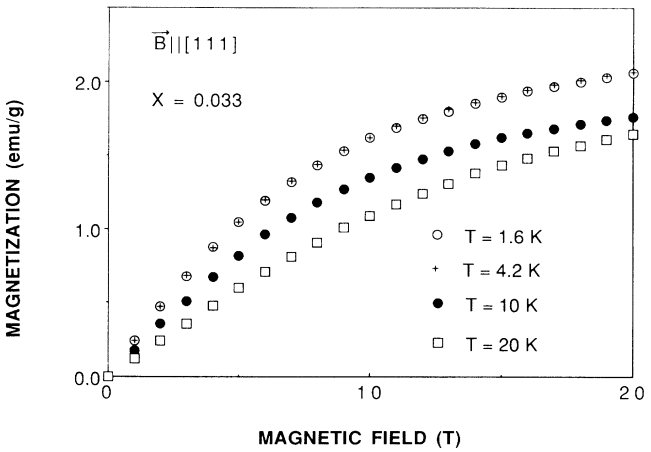

FIG. 3. Same as Fig. 1, for $\mathbf{B}\|[111]$.

have been used to prepare cubic samples ($5\times5\times5$ cm^3) with two oriented surfaces. For one type of sample the two oriented surfaces are in the (110) and (001) planes. For the other type they are in the (110) and ($1\bar{1}1$) planes. Magnetic measurements have been performed on both types of oriented samples with the same Fe concentration, in order to get the magnetization curves for magnetic field **B** applied along the main crystal axes (110), (001), and ($1\bar{1}1$). The homogeneity of the investigated samples has been carefully controlled, not only by microprobe analysis, but also by checking the coincidence of the magnetization curves of both types of oriented samples for $\mathbf{B}\|$ [110].

The magnetization measurements were carried out in the high field magnet laboratory of Grenoble. The magnetic field ($B\leq20$ T) is produced by a "Bitter" resistive magnet, and the magnetometer which allows accurate magnetization measurements is based on the extraction method.[10] The magnetic moment of the sample is deduced from the flux variation induced by a motion of the sample between two pick-up coils. After accurate compensation and positioning of these coils, the signal is integrated by a digital converter. The absolute calibration of the magnetic moment is achieved by using monocrystalline spheres of pure nickel and yttrium garnet as reference samples. The sensitivity of the magnetometer is the order of 5×10^{-4} emu, and the accuracy of the measurements is 2%.

Magnetization measurements have been made for various temperatures in the range $1.5\leq T\leq20$ K. Below 4.2 K, the temperature is fixed by regulating the pressure of the liquid-helium bath. Above 4.2 K, a calorimeter formed of two concentric chambers is introduced into the cryostat, and the sample is placed in the inner chamber filled with helium gas. By pumping the helium gas in the outer chamber, the sample is isolated from the cryogenic bath, and the Joule dissipation of a weak electric resistance (5–50 mW) is sufficient to change the temperature. Carbon resistors are used as thermometers. Similar resistors are used to pilot the temperature regulator.

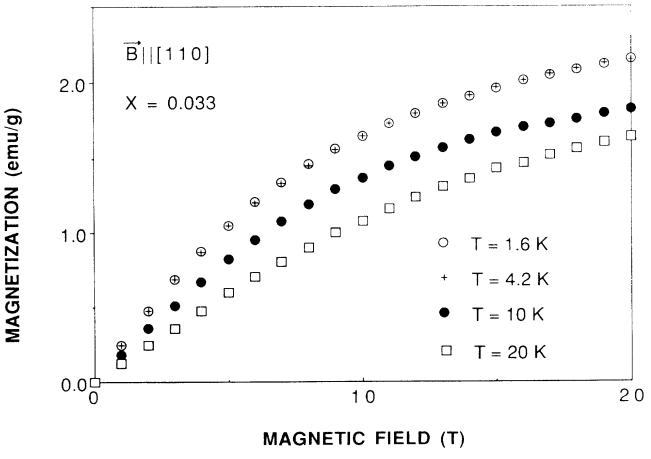

FIG. 2. Same as Fig. 1, for $\mathbf{B}\|[110]$.

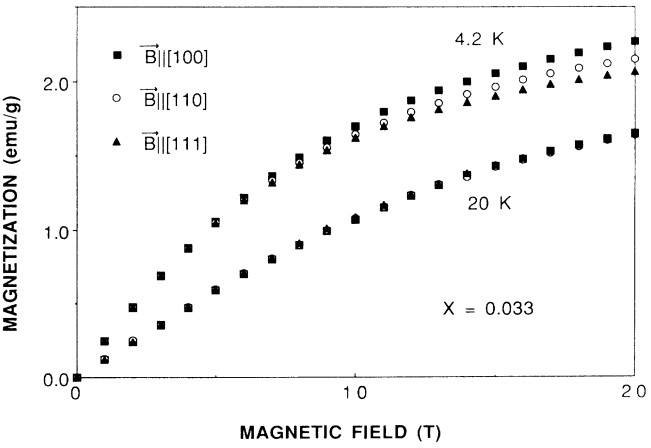

FIG. 4. Experimental magnetization curves of $Cd_{1-x}Fe_xTe$ ($x=0.033$) at $T=4.2$ and 20 K, for **B** along the main crystallographic axes.

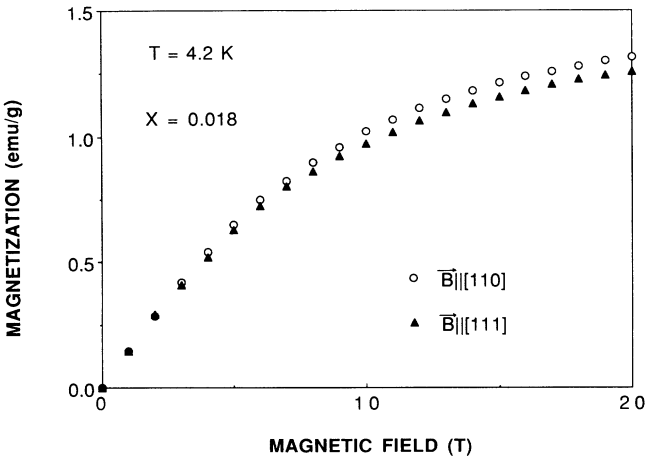

FIG. 5. Experimental magnetization curves of $Cd_{1-x}Fe_xTe$ ($x=0.018$) at $T=4.2$ K for $\mathbf{B}\|[110]$ and [111].

III. EXPERIMENTAL RESULTS

Magnetization curves of $Cd_{1-x}Fe_xTe$ ($x=0.033$) have been measured at $T=1.6$, 4.2, 10, and 20 K. The results are reported in Figs. 1–3 for the magnetic field along the [100], [110], and [111] crystal axes, respectively. The magnetization curves $M(B)$ are the same at 1.6 and 4.2 K, which is evidence of the Van Vleck nature of the paramagnetism. At low magnetic field ($B<2$ T), M varies linearly as a function of B, and the susceptibility $\chi=M/B$ is independent of the orientation of $\mathbf{B}$, a property resulting from the cubic structure of $Cd_{1-x}Fe_xTe$. At higher fields, the magnetization curves $M(B)$ deviate from the linearity, and a magnetic anisotropy appears above $B=5$ T, with the easy axis in the [100] direction. This feature is illustrated in Fig. 4, which shows the $M(\mathbf{B})$ curves of the $x=0.033$ sample, for $\mathbf{B}\|[100]$, [110], and [111]. Similar data are reported in Fig. 5 for an $x=0.018$ sample, and $\mathbf{B}\|[110]$ and [111]. The relative variation of $M(B=20\text{ T})$ at $T=4.2$ K is about 4% between the [110] and [111] directions, for both samples, and it reaches about 10% between the [100] and [111] directions. This magnetic anisotropy decreases with increasing temperature above 10 K, and disappears at $T\approx 20$ K, as is shown in Fig. 4 for the $x=0.033$ sample.

IV. THEORETICAL MODEL

A. Magnetization of isolated ions

We start from the crystal-field model reported in Sec. IV of paper I. In the presence of an external magnetic field, the Hamiltonian acting on an isolated Fe^{2+} ion is

$$H'=H+\mu_B(\mathbf{L}+2\mathbf{S})\cdot\mathbf{B}\ , \tag{1}$$

where H is the electronic Hamiltonian (see paper I), and the additional term is the Zeeman interaction. To solve Eq. (1), one can calculate the matrix elements of this Zeeman term in the basis of the 25 states issued from the ^5D ground state. This is the procedure used by Slack, Roberts, and Vallin[3] to solve the problem for $\mathbf{B}\|(100)$. Another possibility is to use our prior work,[5] which we originally developed to study the magnetization curves of $Cd_{1-x}Fe_xSe$,[7] since the Hamiltonian H_{Fe} solved in this reference reduces to Eq. (1), when the trigonal distortion is set equal to zero. The Hamiltonian matrix has been expressed in the basis set $|\psi_i\rangle$ given in table 1 of Ref. 5, which only differs from the basis reported in Tables I and II of paper I by a unitary transformation; in Ref. 5 all the H' matrix elements are given in tables 2, 3, and 4, and the Zeeman matrix is given in tables 5–8, in terms of the parameters $10Dq$, λ, already defined in paper I, and two additional parameters v and v' which are both equal to zero in $Cd_{1-x}Fe_xTe$. This Zeeman matrix has been expressed for any $\mathbf{B}$ in the plane containing [111] and $[\bar{1}\,\bar{1}2]$ directions, in notations where $h_\parallel, h_\perp$ are the projections of B along these two directions, respectively. The [110] direction is in this plane. The [001] direction is also in this plane, and it is equivalent to the [100] axis in $Cd_{1-x}Fe_xTe$ which crystallizes in a cubic structure. Tables 1–8 in Ref. 5 are thus all we need to solve the eigenvalue problem for H', for any magnetic field along the three principal crystal axes considered in the present work. We have also considered the spin-spin interaction H_{ss}, with ρ the spin-spin coupling parameter, as mentioned in paper I. The diagonalization of the 25×25 matrix H' then gives the energy eigenvalues E_i, and the eigenvectors $|\phi_i(\mathbf{B})\rangle$ (which reduce to the $|\tilde{i}\rangle, |\bar{\tilde{I}}\rangle$'s in the limit $B=0$) labeled in increasing order of energy. We actually used both procedures, i.e., solved the eigenvalue problem for the Hamiltonian expressed in both sets of basis functions, and checked that the results obtained are just the same, which is a check of our algebra, and of the algorithm. Then, the magnetic moment μ_i associated to the ith state is

$$\mu_i=-\mu_B\langle\phi_i(\mathbf{B})|(\mathbf{L}+2\mathbf{S})\cdot\mathbf{B}/B|\phi_i(\mathbf{B})\rangle \tag{2}$$

and the magnetization per isolated Fe^{2+} at temperature T is

$$M_1(B)=\left[\sum_{i=1}^{25}\mu_i(B)e^{-E_i/k_BT}\right]\Big/\left[\sum_{i=1}^{25}e^{-E_i/k_BT}\right]. \tag{3}$$

The values of E_i as a function of B have already been reported in Ref. 9 for $\mathbf{B}\|[100]$ and [111] for the 10 states issuing from the ^5E level. For comparison and completeness, we thus only report in Fig. 6 the variations of E_i for these states as a function of $\mathbf{B}\|[110]$. Figure 1 in Ref. 9 and Figure 6 in the present work show that the energy splitting of the excited states strongly depends on the direction of the magnetic field, and the same holds true for the ϕ_i's. As a result, a strong anisotropy of $M_1(B)$ is predicted by the model with upper and lower values of the magnetic moment of isolated Fe^{2+} ions corresponding to $\mathbf{B}\|[100]$ and [111], respectively. We have already studied this anisotropy in our prior work,[9] where the theoretical curves $M_1(B)$ have been computed from Eqs. (2) and (3), with the values $10Dq=-2480$ cm^{-1} and $\lambda=-100$ cm^{-1}. In particular, we have found that the magnetic anisotropy, as measured by $(M_1^{[100]}-M_1^{[111]})/M_1^{[111]}$ in obvious notations, becomes significant above

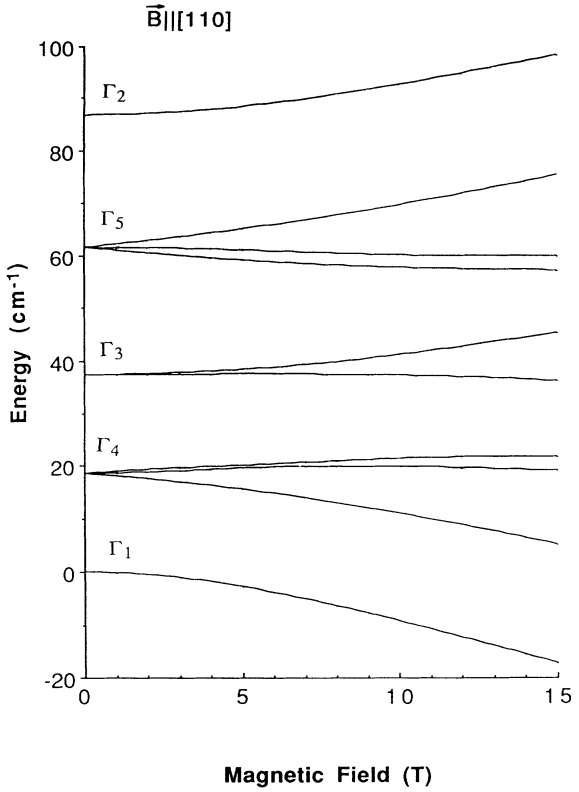

FIG. 6. Spectrum of the five levels of the ^5E states of Fe^{2+} in CdTe for $\mathbf{B}\|[110]$ ($Dq=-248$ cm^{-1} and $\lambda=-100$ cm^{-1}) (Ref. 9).

$B=3$ T, and increases continuously with B, to reach 20% for $B=15$ T at 4.2 K (see Figs. 2 to 5 in Ref. 9), exceeding the experimental value by a factor 2. Therefore, Eqs. (2) and (3) can account for the existence and the sign of the magnetic anisotropy, but fails to give quantitative agreement with experiment.

The above-mentioned values of $10Dq$ and λ are relevant to $Cd_{1-x}Fe_xTe$ only when Jahn-Teller effects are neglected (see paper I). Since we have just shown in paper I that Jahn-Teller effects on the E-orbital states are important to understand the optical properties of this material, one may wonder whether they also play a role in the magnetic properties. We have thus also solved the eigenvalue problem of the Hamiltonian $H'+H_{JT}$, with H_{JT} the Jahn-Teller Hamiltonian of paper I. Focusing on this problem, the Hamiltonian matrix has been expressed in the vibronic basis $|\bar{e},n,m)$ defined in paper I, since we have shown that the H_{JT} matrix is block diagonal in this basis. However, the Zeeman Hamiltonian has the symmetry T_2, different from the symmetry E of H_{JT}. As a consequence, the full Hamiltonian $H'+H_{JT}$, which includes the Zeeman term, is no longer reduced to a block-diagonal form when expressed in the $|\bar{e},n,m)$ basis, as soon as $B\neq 0$. In order to keep the dimension of the matrix we want to diagonalize to a manageable level, we have only kept, as basis states, all 73 $|\bar{e},n,m)$ states which have an energy $E_i+(n+m+1)\hbar\omega\leq 100$ cm^{-1} above that of the ground state $|\bar{a},0,0)$. This truncation implies that some of the excited states are not well described, but the ground eigenstate [which reduces to $|\Gamma_1{:}\bar{a}00)$ for $B=0$] is reproduced nicely, since the quantum mixing of $|\bar{a},0,0)$ with the remote $|\bar{e},n,m)$ states more than 100 cm^{-1} higher in energy is totally negligible. The reason is that, even at the highest magnetic field investigated, i.e., 20 T, the strength of the Zeeman interaction is only of the order of $\mu_B B\approx 1$ meV, and that of the Jahn-Teller interaction is $E_{JT}\approx 0.6$ meV according to paper I, which is one order of magnitude smaller than 100 cm$^{-1}\cong 12.4$ meV. At low temperature $T\leq 10$ K, only the ground state is populated and thus contributes to the magnetization according to the Boltzmann distribution in Eq. (3). A quantitative determination of $M_1(B)$ at $T\leq 10$ K, in the presence of the Jahn-Teller interaction, is thus achieved by the computation of Eq. (3), where the E_i's and ϕ_i's are now the eigenvalues and eigenstates of the 73×73 Hamiltonian matrix $H'+H_{JT}$ in the truncated basis. Note that in such a computation, we must now choose for the spin-orbit constant the Fe^{2+} free-ion value, which, following paper I, must be chosen equal to -101.9 cm^{-1}. We did this calculation in both the [100] and [110] directions, and found that the difference with the former results where the Jahn-Teller effect was neglected is totally negligible (smaller than 1% at all fields), because there is a compensation of the variations of M_1 arising from the introduction of H_{JT} with those arising from the change in the parameter λ. It follows that the discrepancy between theory and the experimental curves is not attributable to a Jahn-Teller effect.

Fe-Fe spin interactions, which we have neglected so far, also contribute efficiently to the magnetization. Since the material is insulating at low temperatures, the magnetic exchange interaction is short range. We can thus, in a first step, restrict it to the NN interaction. The corrections associated with the interaction beyond NN will be included in a second step.

B. Nearest-neighbor exchange interaction

Since we have investigated compounds of low Fe concentration only ($x=0.018$ and 0.033), the probability of finding magnetic clusters of more than two Fe^{2+} ions in the nearest-neighbor (NN) position is negligible, if we assume that the statistical distribution of Fe^{2+} in the matrix is random. Therefore, we will take the NN exchange interaction into account, by including in the calculation of the magnetization the contribution of NN Fe^{2+}-Fe^{2+} pairs only. We can approximate the magnetization per unit mass as the sum of the contributions from isolated Fe^{2+} ions, M_s, and NN Fe^{2+}-Fe^{2+} pairs, M_p, plus the diamagnetic contribution from the lattice:

$$M=M_s+M_p+M_{\text{dia}}\ ,$$
$$M_s=M_1P_1(x)\frac{xN_A}{m(x)},\quad M_p=\tfrac{1}{2}M_2P_2(x)\frac{xN_A}{m(x)}\ . \tag{4}$$

M_1 is expressed in Eq. (2). M_2 is the magnetic moment of a NN Fe^{2+}-Fe^{2+} pair. $P_1(x)$ is the probability that an Fe^{2+} ion has no NN. $P_2(x)$ is the probability that an Fe^{2+} ion belongs to a pair. For a random distribution of

iron ions on the cation sublattice, we have

$$P_1(x)=(1-x)^{12} ,$$

$$P_2(x)=12x(1-x)^{18} .$$

N_A is the Avogadro number and $m(x)$ is the molar mass of $Cd_{1-x}Fe_xTe$. Finally, $M_{dia}=-\chi_{CdTe}B$, with $\chi_{CdTe}=-3.45\times10^{-7}$ emu/g.

To determine M_2, we assume that the exchange interaction is of the Heisenberg type, i.e., we write the interaction between two NN Fe^{2+} spins S_1,S_2 under the form

$$H_{NN}=-2\mathbf{J}\mathbf{S}_1\cdot\mathbf{S}_2 . \quad (5)$$

Since we have already solved the eigenvalue and eigenvector problems for the Hamiltonian H' of an isolated ion in the preceding section, it is convenient to express the pair Hamiltonian matrix in the basis $|\phi_i\phi_m\rangle$, which represents the direct product of the wave function ϕ_i relative to the magnetic ion labeled 1 in Eq. (5), by the wave function ϕ_m relative to the magnetic ion labeled 2. Again, the 10 lower electronic states $\phi_i(B)$ of one isolated Fe^{2+} ion, issuing from the ^5E level, are separated from the 15 other states by the energy $10Dq$, which is orders of magnitude larger than the exchange constant J. Therefore, the coupling induced by H_{NN} between the states ϕ_i, with $i\leq10$, and ϕ_j, with $j>10$ of a given Fe^{2+} ion, due to the presence of a nearest neighbor, is negligible. Moreover, the 15 higher states are not occupied at the temperatures of interest. Therefore, only the intracoupling within the ^5E ground configuration must be considered. We have then calculated the matrix elements of the pair Hamiltonian in the truncated basis $|\phi_i\phi_m\rangle$, where the indices i and m only scan integers in the range [1,10]. Note that we take explicitly into account the ^5E-$^5T_2$ mixing generated by the spin-orbit coupling (and incidentally by the magnetic field too; this one is also very small), since the $|\phi_i\rangle$'s are eigenstates of the matrix H' in the basis which includes both the $|\tilde{e}\rangle$ and the $|\tilde{T}\rangle$ states. Only the ^5E-$^5T_2$ mixing generated by H_{NN} is neglected in the process, which is meaningful because, as we shall see, the exchange constant J is small compared with the spin-orbit constant λ.

From a numerical point of view, we proceed as follows. The spin matrices have been reported in the $|\psi_i\rangle$ basis in tables 9 and 10 in Ref. 5. The decomposition of the $|\phi_i\rangle$'s in the $|\psi_i\rangle$ basis is obtained as a result of the diagonalization of the 25×25 matrix H' displayed in tables 1–8 in Ref. 5. It is then straightforward to compute the matrix elements $\langle\phi_i|\mathbf{S}|\phi_m\rangle$ from tables 9 and 10 in Ref. 5, which gives the matrix elements of $\mathbf{S}$ in the $|\psi_i\rangle$ basis. Then the 100×100 Hamiltonian matrix H_{NN} is computed in the set $|\phi_i\phi_m\rangle$ $(i,m\in[1,10])$, and diagonalized. Then $M_2(B)$ is computed from Eqs. (2) and (3), where E_i and $|\phi_i\rangle$ are now replaced by the eigenvalues and eigenvectors of H_{NN}. The computations have been performed for different values of J, for magnetic fields applied along the three main crystallographic axes [100], [110], and [111]. The results thus obtained are found in agreement with the calculations of Fe^{2+}-Fe^{2+} NN pairs performed by Twardowski[11] in this material. They are illustrated in Fig. 7, which shows the magnetization curves $M_2(\mathbf{B})$ of an Fe-Fe pair computed for several values of the NN exchange constant, in the case $T=4.2$ K, $\mathbf{B}\|[100]$. For $J=0$, $M_2(\mathbf{B})$ reduces to $2M_1(\mathbf{B})$. As the strength of the exchange coupling increases, the pair magnetization decreases, and a change of the curvature appears in the $M_2(\mathbf{B})$ curve: the curvature, negative for small $|J|$ (like that of the magnetization of isolated ions) increases with $|J|$, and changes sign for $J=-3.75$ K. For comparison, we have illustrated in Fig. 8 both theoretical magnetization curves $M_1(\mathbf{B})$ and $M_2(\mathbf{B})/2$ relative to an isolated and a coupled ion, for $\mathbf{B}\|[100]$ and [111], at $T=4.2$ K, for $J=-8.8$ K. Note that the magnetic anisotropy of $M_2(\mathbf{B})$ is weaker, and of opposite sign with respect to that of $M_1(\mathbf{B})$, i.e., $M_2^{[111]}\geq M_2^{[100]}$ for a given $|\mathbf{B}|$.

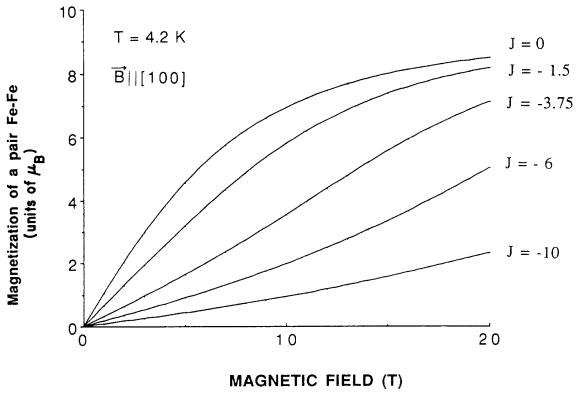

FIG. 7. Theoretical magnetic moment of an Fe^{2+}-Fe^{2+} pair for several values of the NN exchange constant J, in the case $\mathbf{B}\|[100]$, at 4.2 K. The crystal-field parameter, the spin-orbit, and the spin-spin constants are $Dq=-248$ cm^{-1}, $\lambda=-97.7$ cm^{-1}, and $\rho=0.18$ cm^{-1}, respectively.

C. Longer-range exchange interactions

Magnetic interactions between magnetic ions are not restricted to nearest neighbors. To take this effect into

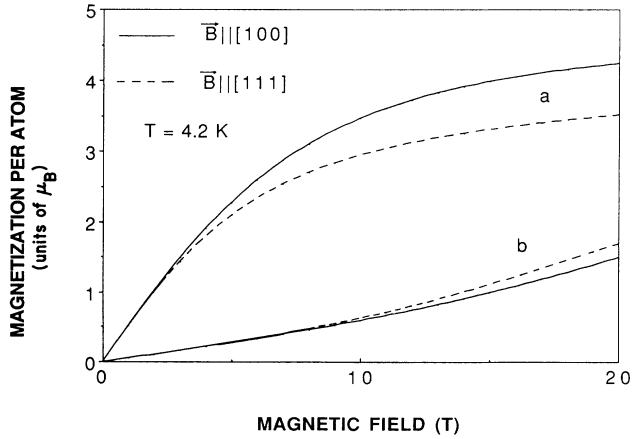

FIG. 8. Theoretical magnetic moment per Fe^{2+} ion at 4.2 K for $\mathbf{B}\|[100]$ and [111], for an isolated ion (a), and a partner of a NN Fe^{2+}-Fe^{2+} pair, with exchange constant $J=-8.8$ K.

account, we add, to the Hamiltonian, the term

$$H_{1g}=-\frac{J'}{N}\sum_{i,j}{}'\mathbf{S}_i\cdot\mathbf{S}_j \tag{6}$$

to describe the long-range part of the exchange interaction, with an effective coupling constant J'. The prime symbol means that nearest neighbors are excluded from the summation over the Fe^{2+} spins, in number N. We treat H_{1g} in the mean-field approximation (MFA), which is known to be reliable for long-range interactions. Assuming again that the Fe^{2+} distribution is random, Eq. (6) takes the form

$$H_{1g}=-\frac{J'}{N}\sum_{i,j}{}'S_i\cdot\langle\mathbf{S}_j\rangle=-xP_1(x)J'\langle\mathbf{S}\rangle\cdot\sum_i\mathbf{S}_i\ . \tag{7}$$

In the preceding expression, we have taken advantage of the fact that $\langle\mathbf{S}_j\rangle$, which is the thermal average of the operator $\mathbf{S}$ in the canonic ensemble, does not depend on the site j. Equation (7) can be combined with H' to give a one-ion effective Hamiltonian:

$$\begin{aligned}&H_{\text{eff}}=H'-I\langle\mathbf{S}\rangle\cdot S\ ,\\&I=xP_1(x)J'\ ,\\&\langle\mathbf{S}\rangle=\left[\sum_{i=1}^{25}\langle\Phi_i(\mathbf{B})|\mathbf{S}|\Phi_i(\mathbf{B})\rangle e^{-\varepsilon_i/k_BT}\right]\Big/\left[\sum_{i=1}^{25}e^{-\varepsilon_i/k_BT}\right].\end{aligned} \tag{8}$$

$|\psi_i(B)\rangle$ and ε_i are the eigenstates and eigenvalues of the matrix H_{eff}. The $\langle\mathbf{S}\rangle$ term of H_{eff} depends on the solution, which is thus found by interaction. In practice, the 25×25 H_{eff} matrix is expressed in the $|\psi_i\rangle$ basis in tables 1–10 of Ref. 5, for a given $\langle\mathbf{S}\rangle$. We start the iteration process from the initial guess $\langle\mathbf{S}\rangle=0$, then solve the eigenvalue problem of H_{eff}. In this first step, H_{eff} is reduced to H', so at the next step $\langle\mathbf{S}\rangle$ is given by Eq. (8), with $|\Phi_i(\mathbf{B})\rangle$ and ε_i replaced by $|\phi_i(\mathbf{B})\rangle$ and E_i. H_{eff} is then diagonalized with this new estimation of $\langle\mathbf{S}\rangle$, and so on, until self-consistency has been reached. Then, the magnetization $M_1(\mathbf{B})$ entering Eq. (4) is computed from relations (2) and (3), in which $|\phi_i(\mathbf{B})\rangle$ and E_i are replaced by $|\Phi_i(\mathbf{B})\rangle$ and ε_i, respectively.

An illustration of the influence of the exchange field on the magnetization of a single Fe^{2+} ion is presented in Fig. 9. Here, the computations have been performed for $T=4.2$ K, and $\mathbf{B}\|[110]$, taking $I=-1.6$ K and $I=0$. The magnetization is reduced by the antiferromagnetic exchange interactions for any value of $\mathbf{B}$, but the effect is more pronounced at intermediate magnetic fields where the curvature of the magnetization curve is large (in absolute value).

V. ANALYSIS

The experimental data can be accurately interpreted only if both the NN-pair interaction and the more-distant-pair exchange interactions are included. This is demonstrated in Fig. 10 by comparing the contribution M_s+M_{dia} of the isolated ions, computed for $I=J=0$, with the experimental curve obtained for a sample of composition $x=0.033$ at $T=4.2$ K, for $\mathbf{B}\|[110]$. A

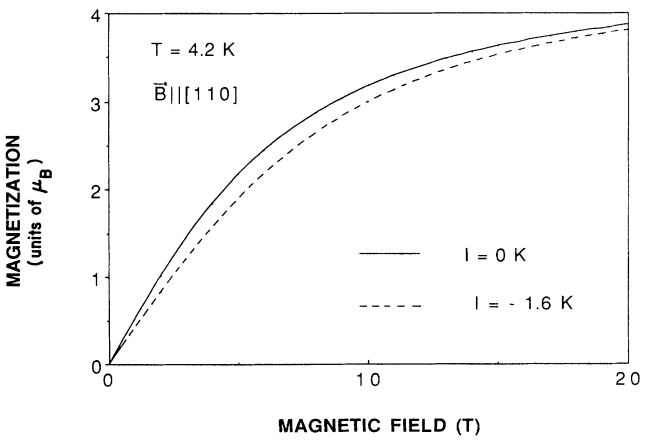

FIG. 9. Theoretical magnetic moment per Fe^{2+} ion at 4.2 K for $\mathbf{B}\|[110]$. The solid line is computed from Eq. (3) ($I=0$). The dashed line is computed from Eq. (8) (see the text) using $I=-1.6$ K, $Dq=-248$ cm^{-1}, $\lambda=-97.7$ cm^{-1}, and $\rho=0.18$ cm^{-1}.

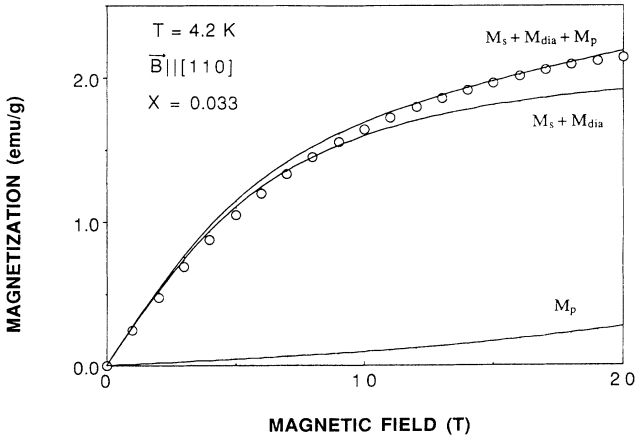

FIG. 10. Comparison between experimental (open circles) and theoretical magnetization curves, for $\mathbf{B}\|[110]$ at $T=4.2$ K. (a) Magnetization M_s+M_{dia} of the isolated ions (including the diamagnetic contribution from the lattice), after Eq. (3) of the test. (b) Contribution of NN Fe^{2+}-Fe^{2+} pairs, M_p, computed for $J=-8.8$ K. (c) Total magnetization $M_s+M_{\text{dia}}+M_p$.

good agreement is found for the low-field susceptibility, but the theoretical curve fails to reproduce the experimental one in the high-field region. The calculated values M_s+M_{dia} are systematically smaller than the experimental data, and overestimate the saturation of the magnetization curve. The contribution M_p of the NN pairs has been computed for different values of the exchange constant J. For the sample of composition $x=0.033$, the best fit between theory and experiments is achieved for $J=-8.8$ K. The magnetization curve $M_s+M_{dia}+M_p$, computed for this value of J (but still $I=0$), is also reported in Fig. 10. The result is an obvious improvement with respect to M_s+M_{dia} alone; now the whole magnetization curve is reproduced nicely at high fields, but still small deviations with respect to the data are found below 12 T. They are eliminated when the more distant magnetic ions are taken into account. This is evidenced in Fig. 11, which shows that an excellent agreement between theory and experiment is found for $J=-8.8$ K, $I=-1.4$ K for these particular conditions ($x=0.033$, $\mathbf{B}\|[110]$).

A complete analysis of the 4.2-K experimental data has been achieved for both compounds ($x=0.018$ and 0.033), taking the exchange constants I and J as fitting parameters. The best fit is achieved for the set of parameters $J=-8.8$ K in both samples, $I=-1.4$ K for $x=0.033$ and $I=-0.8$ K for $x=0.018$%. This fit is illustrated in Figs. 11, 12, and 13. For $x=0.018$, an excellent agreement between theory and experiments is found for $\mathbf{B}\|[110]$ and [111] (experimental data along [100] are not available for this compound). For $x=0.033$, an excellent agreement is still found for $\mathbf{B}\|[110]$ and [100], but discrepancies, the order of 5%, exist for $\mathbf{B}\|[111]$. Since these discrepancies are observed only for the sample which has the highest value of x, they may be attributable to the contribution of larger clusters (triplets, etc.) which

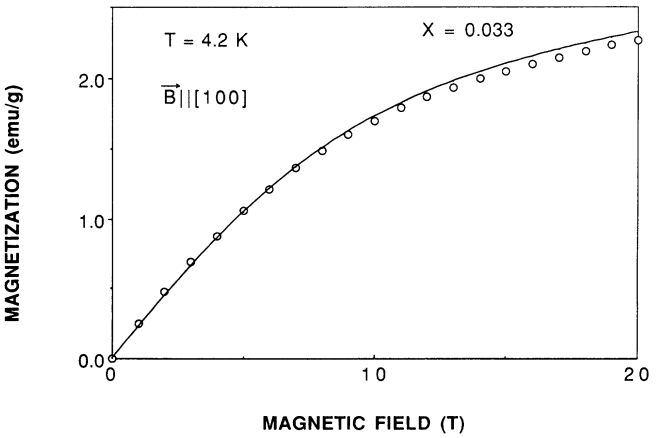

FIG. 12. Comparison between theoretical and experimental magnetization curves of $Cd_{1-x}Fe_xTe$ ($x=0.033$), for $T=4.2$ K and $\mathbf{B}\|[100]$. Open circles are experimental data. The solid line is theoretical, including the pair magnetization ($J=-8.8$ K) and the long-range antiferromagnetic interaction ($I=-1.4$ K).

are neglected in the model. Note that J has been found independent of x, in agreement with the model. On the other hand, for a random distribution, the exchange constant I is expected to satisfy the relation

$$I=12x(1-x)^8[J_2+4J_3(1-x)^2] ,$$

where J_2 and J_3 are the second- and third-neighbor exchange constants. The above-mentioned values of I for $x=0.018$ and 0.033 are quite consistent with the above relation if we note that the x dependence of the term in J_3 is negligible for such low concentrations.

We have explored the uniqueness of the solution for the set of parameters (I,J) and found that a good agree-

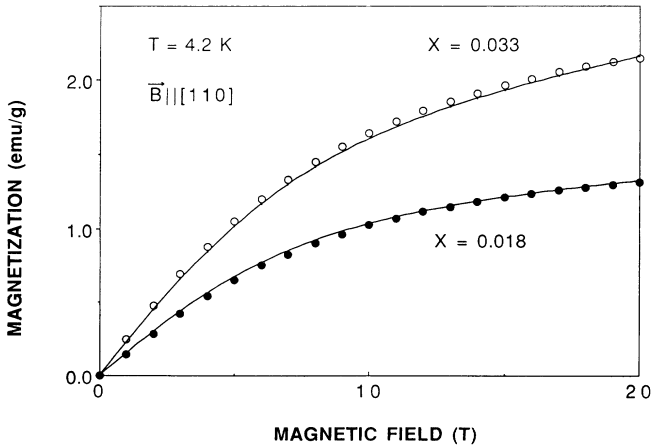

FIG. 11. Comparison between theoretical and experimental magnetizations for $\mathbf{B}\|[110]$ at $T=4.2$ K. The data are reported in black symbol for the $x=0.018$ sample and open circles for the $x=0.033$ sample. The solid lines are calculated from our model, including the pair contribution ($J=-8.8$ K) and the long-range antiferromagnetic interactions, with exchange constant $I=-0.8$ K for $x=0.018$ and $I=-1.4$ K for $x=0.033$.

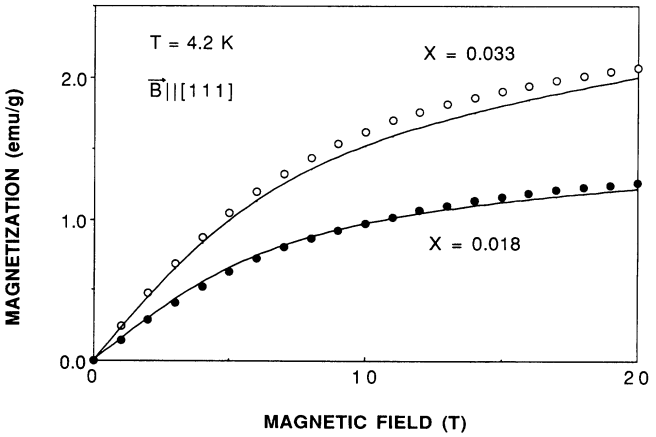

FIG. 13. Comparison between theoretical and experimental magnetization curves of $Cd_{1-x}Fe_xTe$, for $T=4.2$ K and $\mathbf{B}\|[111]$. Black and open circles are experimental data for $x=0.018$ and 0.033, respectively. The solid line is theoretical, including the pair magnetization ($J=-8.8$ K) and the long-range antiferromagnetic interaction with $I=-0.8$ K for $x=0.018$ and $I=-1.4$ K for $x=0.033$.

ment with experiments exists for values of J which range from $J=-8.8$ to -7.5 K, in which case $I=-1.0$ and -1.6 K for $x=0.018$ and 0.033, respectively. This allows an estimate of the accuracy with which the values of I and J have been determined from the analysis of our data:

$$J=-8.8\pm1.2 \text{ K} ,$$

$$J_2+4J_3\approx\frac{I}{12x(1-x)^8}=-5\pm0.5 \text{ K} .$$

Finally, the values of the p-d exchange constant ($N_0\mu_B$ in conventional notation) are known to be large and negative: $N_0\mu_B=-1.27\pm0.08$ eV in $Cd_{1-x}Fe_xTe$,[12] compared with the value -0.88 eV in $Cd_{1-x}Mn_xTe$.[13] This is already an indication that the hybridization of the d states of Fe^{2+} with the Γ_8 band is large. A second manifestation of this effect is the large value of the NN exchange constant $J=-8.8$ K in $Cd_{1-x}Fe_xTe$, against -6.3 K in $Cd_{1-x}Mn_xTe$. Note that the exchange parameters we found in $Cd_{1-x}Fe_xTe$ are close to those met for Mn^{2+} ions in $Cd_{1-x}Mn_xTe$.[14]

ACKNOWLEDGMENTS

The authors gratefully acknowledge Madame N. Valignat, from Institut National Polytechnique (Grenoble), who made the electron microprobe analysis.

*Permanent address: Institute of Physics, Polish Academy of Sciences, Al. Lotnikow 32, Warsaw, Poland.

[1]A. Mycielski, J. Appl. Phys. **63**, 3279 (1988).
[2]A. Twardowski, J. Appl. Phys. **67**, 5108 (1990).
[3]G. A. Slack, S. Roberts, and J. T. Vallin, Phys. Rev. **187**, 511 (1969).
[4]J. P. Mahoney, C. C. Lin, and F. Dorman, J. Chem. Phys. **53**, 4286 (1970).
[5]A. Mauger, D. Scalbert, J. A. Gaj, J. Cernogora, and C. Benoit à la Guillaume, Solid State Commun. **69**, 453 (1989).
[6]D. Scalbert, J. Cernogora, A. Mauger, C. Benoit à la Guillaume, and A. Mycielski, J. Cryst. Growth **101**, 940 (1990).
[7]D. Scalbert, M. Guillot, A. Mauger, J. A. Gaj, J. Cernogora, C. Benoit à la Guillaume, and A. Mycielski, Solid State Commun. **76**, 977 (1990).
[8]A. Twardowski, K. Pakula, I. Perez, P. Wise, and J. E. Crow, Phys. Rev. B **42**, 7567 (1990).
[9]C. Testelin, A. Mauger, C. Rigaux, M. Guillot, and A. Mycielski, Solid State Commun. **71**, 923 (1989).
[10]J. C. Picoche, M. Guillot, and A. Marchand, Physica B **155**, 407 (1989).
[11]H. J. M. Swagten, A. Twardowski, W. J. M. de Jonge, and M. Demianuk, Phys. Rev. B **39**, 2568 (1989), and references therein.
[12]C. Testelin, C. Rigaux, A. Mycielski, and M. Menant, Solid State Commun. **78**, 659 (1991).
[13]J. A. Gaj, R. Planel, and G. Fishman, Solid State Commun. **29**, 435 (1979).
[14]Y. Shapira and N. F. Oliveira, Phys. Rev. B **35**, 6888 (1987).